Branching Structures in Elastic Shape Optimization

Nora Lüthen [*] Martin Rumpf [†] Sascha Tölkes [†]
Orestis Vantzos [‡]

November 13, 2017

Abstract

Fine scale elastic structures are widespread in nature, for instances in plants or bones, whenever stiffness and low weight are required. These patterns frequently refine towards a Dirichlet boundary to ensure an effective load transfer. The paper discusses the optimization of such supporting structures in a specific class of domain patterns in 2D, which composes of periodic and branching period transitions on subdomain facets. These investigations can be considered as a case study to display examples of optimal branching domain patterns.
In explicit, a rectangular domain is decomposed into rectangular subdomains, which share facets with neighbouring subdomains or with facets which split on one side into equally sized facets of two different subdomains. On each subdomain one considers an elastic material phase with stiff elasticity coefficients and an approximate void phase with orders of magnitude softer material. For given load on the outer domain boundary, which is distributed on a prescribed fine scale pattern representing the contact area of the shape, the interior elastic phase is optimized with respect to the compliance cost. The elastic stress is supposed to be continuous on the domain and a stress based finite volume discretization is used for the optimization. If in one direction equally sized subdomains with equal adjacent subdomain topology line up, these subdomains are consider as equal copies including the enforced boundary conditions for the stress and form a locally periodic substructure.
An alternating descent algorithm is employed for a discrete characteristic function describing the stiff elastic subset on the subdomains and the solution of the elastic state equation. Numerical experiments are shown for compression and shear load on the boundary of a quadratic domain.

Key Words: Shape optimization, elasticity, branching patterns

[*]Chair of Computational Science, Clausiusstrasse 33, ETH-Zentrum, CLT C 14, 8092 Zürich, Switzerland, nluethen@ethz.ch
[†]Institute for Numerical Simulation, University of Bonn, Endenicher Allee 60, 53115 Bonn, Germany, {martin.rumpf}{sascha.toelkes}@ins.uni-bonn.de
[‡]Center for Graphics and Geometric Computing (CGGC), Computer Science Department, Technion, Technion City, Haifa, 32000, Israel, vantzos@cs.technion.ac.il

1 Introduction

The formation of microstructures is a common phenomenon in elastic shape optimization. We refer to [2] and [1] for an overview about these topics. Depending on the geometry of the computational domain and the loads applied to it different type of microstructures appear. In fact, besides locally periodic structures one also observes branching type patterns when optimizing with respect to a compliance cost functional, a volume cost, and the perimeter of the structure. These patterns refine towards a Dirichlet boundary of the configuration [17, Figure 13]. Such branching patterns can also been observed in nature, for instance in the spongiosa of bones [14]. For the basic load configurations of uniaxial load and shear load Kohn and Wirth [9, 10] considered scaling laws for the cost functional and for the weight in front of the perimeter tending to zero.

Besides the question how locally periodic or branching periodic patterns might look like, a central challenge is also to identify optimal decompositions of elastic material devices or objects into such spatially varying patterns. This paper should be regarded as a case study in this direction. It is intended as a first step towards a truely multiscale modeling of optimized elastic objects involving periodic and branching periodic patterns. Such a multiscale model would enable to apply techniques from *homogenization*, an important concept to upscale the microscopic properties to a macroscale. This methodology has been described for instance in [4, 12] and in detail in the context of elastic shape optimization in [1] and in the context of engineering applications for instance in [15] and [16]. Two-scale materials can be numerically computed by the Heterogeneous Multiscale Method (HMM) [6, 5, 7, 8], which explicitly simulates periodic microstructures at positions in the macroscopic domain.

Here we consider domain patterns which explicitly prescribe locally periodic or branching periodic structures on a fine scale instead of taking into account a truely multiscale model. To this end we study computational domains that can be decomposed into a set of rectangular subdomains with compatibility conditions on the facets of these domains. The actual elastic structure will be a subset of the computational domain, which we aim to identify via elastic shape optimization. This elastic structure correspondingly splits into components on the subdomains. Each subdomain will be a copy of one rectangular reference cell on which the shape of a hard phase will be optimized. Then these elastic structures in the subdomains assemble to a locally periodic or a locally branching type structures. The discretization discussed in this article is an extension of the approach suggested by one of the authors, O. Vantzos and also used in [11], now going beyond purely branching periodic ensembles of cells.

The paper is organized as follows: in Section 2 we describe the admissible subdivision of the computational domain into cells. Then, Section 3 discusses the underlying elasticity model and the optimization problem. Section 4 presents the spatial discretization and the numerical solution of the state equation, whereas in Section 5 the alternating descent scheme for the optimization of the discrete characteristic function is investigated. Finally, results for two different load configurations are depicted in Section 6.

2 Composite structures

Let $D \in \mathbb{R}^2$ be a computational domain consisting of several subdomains D_i, $i = 1, \ldots, M$ for some $M \in \mathbb{N}$, such that $\cup_{i=1}^{M} \overline{D_i} = D$ and $\cap_{i=1}^{M} D_i = \emptyset$. Each subdomain ist supposed to be a rectangle $(a_1, a_2) \times (b_1, b_2)$. Each facet of a subdomain

(i) is either also a facet of an adjacent subdomain (e.g. there is a subdomain $(a_2, a_3) \times (b_1, b_2)$ sharing the facet $\{a_2\} \times (b_1, b_2)$ with the subdomain $(a_1, a_2) \times (b_1, b_2)$),

(ii) or splits into two facets of two adjacent subdomains (e.g. there are subdomains $(a_2, a_3) \times (b_1, \frac{b_1+b_2}{2})$ and $(a_2, a_3) \times (\frac{b_1+b_2}{2}, b_2)$ whose facets $\{a_2\} \times (b_1, \frac{b_1+b_2}{2})$ and $\{a_2\} \times (\frac{b_1+b_2}{2}, b_2)$ results from a splitting of the facet $\{a2\} \times (b_1, b_2)$),

(iii) or is on the facets resulting from such a splitting of a facet of an adjacent subdomain,

(iv) or is a boundary facet.

We always assume that the splitting of facets is in two halves of equal length. The subdomain configurations at a single facet are shows in Figure 1. The four facets of a single rectangular subdomain can be of different type.

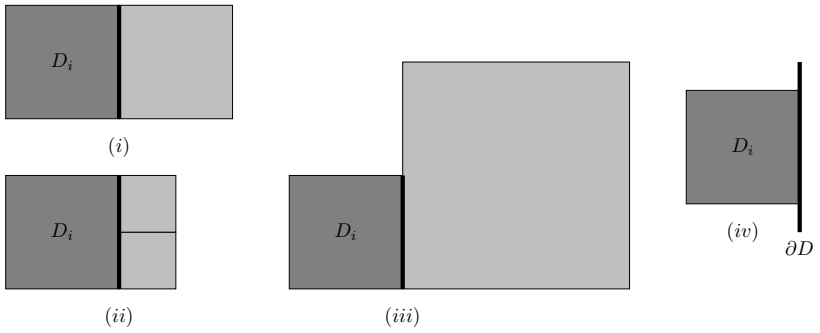

Figure 1: The different local subdomain configurations at a single facet.

Let us assume that each subdomain D_i contains an inscribed subpart of the actual elastic object, the shape of which will be optimized. Let us denote by χ_i the associated characteristic function. for which we consider the continuous extension in BV onto the closure of the subdomain. Thus, $\sum_{i=1}^{M} \chi_i$ as function on $\overline{D}$ is the characteristic function of the elastic objects we are investigating. Each (geometric) subdomain D_i will have a reference domain assigned and several geometric subdomains can have the same reference domain. The referenced domain is mapped onto a geometric subdomain via a translation and a rotation by a multiple of $\frac{\pi}{2}$. The characteristic function χ_i and later also the force distribution on $[\chi_i = 1]$ is handled and updated on the associated reference domain. Thus, the computational complexities scales with the number of

reference domains. If adjacent subdomains share the same reference domain and the same rotation, then they are building blocks of local, period elastic structures. Fig. 2 illustrates such a domain decomposition into rectangular boxes.

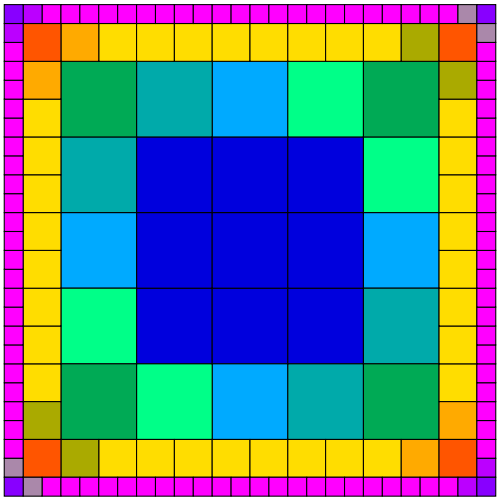

Figure 2: An examplary decomposition of the computational domain is displayed with 13 different reference domains that are mapped to the subdomains of the decomposition, where identical colors classify the different reference domains. The different types are locally periodic cells (■), branching cells (■ ■ ■), double branching corner cells (■ ■ ■) and coupling cells (■ ■ ■ ■ ■ ■).

As a consequence, the domain sketched in Figure 2 can later be numerically optimized by a shape optimization on 13 (coupled) reference domains only.

3 Elastic state equation and compliance optimization

To solve the elastic state equation in the context of the shape optimization we use the quadratic energy of a stress based formulation of linearized elasticity. On the same basis we evaluate the compliance-type target functional. On each reference domain the shape will be modelled by a phase field $v : D_i \to \mathbb{R}$ where v is assumed to approximate the characteristic function of the elastic object χ. Thus, $\{x \in D_i \,|\, v(x) \approx 1\}$ corresponds to the actual elastic domain and $\{x \in D_i \,|\, v(x) \approx 0\}$ to the void (or in our calculation very soft) phase.

Let us consider elastic stresses $\tau : D_i \to \mathbb{R}^2$ as extensions of the elastic stresses on the elastic object $[\chi = 1]$. Let us recall that stresses act on normals of infinitesimal area elements and represent the force density acting on this area element. We apply solely boundary forces and no volume forces. Hence, elastic stresses are divergence free, which constitutes together with the boundary condition the state equation of our optimization problem. Given the elasticity tensor $C(v)$, which depends on the phase

(hard or soft) the stored elastic energy elastic on D_i is defined as

$$\mathcal{E}[v,\tau] = \int_{D_i} \mathcal{C}^{-1}(v)\tau : \tau \,\mathrm{d}x\,. \tag{3.1}$$

Here $\mathcal{C}(v)$ is a fourth order tensor satisfying $\mathcal{C}_{ijkl}(v) = \mathcal{C}_{jikl}(v) = \mathcal{C}_{ijlk}(v) = \mathcal{C}_{klij}(v)$. In the context of this paper, we define

$$\mathcal{C}(v) = v\mathcal{C}_{NL}$$

where $\mathcal{C}_{NL}$ is the elasticity tensor of the linearized Navier-Lamé elasticity model and $\delta > 0$. We define the inverse $\mathcal{C}^{-1}$ (needed in (3.1)) using *Young's modulus* E and the Poisson ratio ν (in Voigt notation)

$$\mathcal{C}_{NL}^{-1} = \frac{1}{E}\begin{pmatrix} 1 & -\nu & 0 \\ -\nu & 1 & 0 \\ 0 & 0 & 2+2\nu \end{pmatrix}.$$

For the phase field function v we consider a Modica Mortola type functional (cf. [13])

$$\mathcal{L}^{\varepsilon}[v] = \int_{D_i} \frac{1}{\varepsilon} W(v) + \frac{\varepsilon}{2} \left|\bigtriangledown v\right|^2 \,\mathrm{d}x$$

which approximates the length of the interface between hard and soft material. Here,

$$W(v) = \begin{cases} \frac{32}{\pi^2}(1-v)(v-\delta) & v \in [\delta, 1] \\ \infty & \text{else} \end{cases}$$

denotes a double-well potential, i. e. a positive function that is attending its only two minima at the pure phases $v = \delta$ and $v = 1$. We assume that $v|_{\partial D}$ is prescribed and describes the imposed fine scale structure on the domain boundary. The parameter ϵ is proportional to the width of the diffused interface. Futhermore, given the phase field v we can easily compute an approximation of the area of the elastic object $\mathcal{V}^{\varepsilon}[v] = \int_{D_i} v(x)\,\mathrm{d}x$.

Combining the energies above, we obtain the objective functional

$$\mathcal{J}[v] = \min_{\tau \in \Sigma_{\mathrm{ad}}} \mathcal{E}[v,\tau] + \beta\mathcal{V}^{\varepsilon}[v] + \eta\mathcal{L}^{\varepsilon}[v]\,, \tag{3.2}$$

of our constraint optimization problem, where the stress τ is minized over the set of admissable stresses

$$\Sigma_{\mathrm{ad}} = \{\sigma : D_i \to \mathbb{R}^{2,2} \,|\, \sigma = \sigma^T, \mathrm{div}\,\sigma = 0, \text{b.c.}\}\,. \tag{3.3}$$

Here, the boundary condition (b.c.) differs for facets on ∂D and for interior facets, where the stresses are continuous across the facet. For facets on ∂D we prescribe forces f with $\tau(x)\cdot n(x) = f(x)$ if $v(x) = 1$. Here, $n(x)$ denotes the outer normal at points $x \in \partial D$.

As in [9, 10], we consider the case of a vanishing Poisson ratio $\nu = \frac{\lambda}{2(\lambda+\mu)} = 0$. As expressed by Kohn and Wirth in [9], this restriction is not expected to have a strong influence because for truss-like structures the lateral contraction is less relevant. The tensor $\mathcal{C}^{-1}$ then reduces to

$$\mathcal{C}_{NL}^{-1} = \frac{1}{E}\begin{pmatrix} 1 & 0 & 0 \\ 0 & 1 & 0 \\ 0 & 0 & 2 \end{pmatrix} .$$

Thus, we obtain for the stored elastic energy on the subdomain D_i

$$\mathcal{E}[v,\tau] = \int_{D_i} \frac{1}{v\,E}(\tau_{11}^2 + \tau_{22}^2) + \frac{2}{v\,E}\tau_{12}^2 \,\mathrm{d}x = \int_{D_i} \frac{1}{v\,E}|\tau|^2 \,\mathrm{d}x\,.$$

In what follows we choose $E = 1$.

4 Discretization

In this section, we present a finite volume discretization of the state equation and discuss the optimization algorithm. For details we refer to [11]. To this end, the conditions for σ prescribed in the set of admissible stress fields Σ_{ad} in (3.3) have to be transcribed into a linear system of equations resulting from the finite volume discretization. For a subdomain D_i we consider a finite decomposition of D_i into $N \times N$ rectangular cells $\mathbf{C}$ of equal size. The discrete forces are defined as constant vectors in $\mathbb{R}^2$ on edges and the discrete phase field is assumed to be constant on cells. As degrees of freedom we consider average forces across edges f_j which approximate

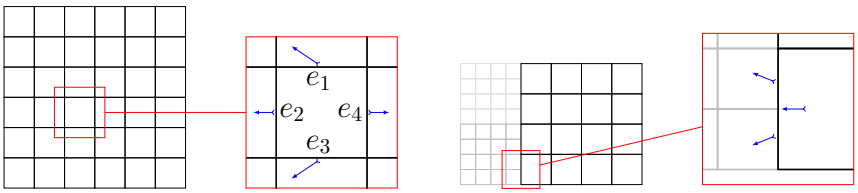

Figure 3: Discretization of forces as vector valued degrees of freedom on the interior cells of the finite volume grid (left) and on a facet with prescribed branching-type boundary conditions (right). The numbering of the edges is displayed on the left.

$\frac{1}{h_j}\int_{\mathbf{e}_j} \sigma \cdot n_j \,\mathrm{d}l$ of a volume cell $\mathbf{C}$ with edge length h_j. (cf. Fig. 3 for a sketch). The symmetry of the stress tensor is transformed into a conservation of torque:

$$\begin{aligned} 0 &= \int_{\partial\mathbf{C}} x \times (n\cdot\sigma)\,\mathrm{d}l = \int_{\partial\mathbf{C}} n\cdot(\sigma x^{\perp})\,\mathrm{d}l = \int_{\mathbf{C}} \mathrm{div}(\sigma x^{\perp})\,\mathrm{d}x \\ &= \int_{\mathbf{C}} \mathrm{div}\sigma\, x^{\perp} + \sigma^T : \bigtriangledown x^{\perp}\,\mathrm{d}x = \int_{\mathbf{C}} \sigma_{21} - \sigma_{12}\,\mathrm{d}x\,, \end{aligned}$$

with $x = (x_1, x_2)$ and $x^\perp = (-x_2, x_1)$ for $\operatorname{div} \sigma = 0$. The conservation law $\operatorname{div} \tau = 0$ in the continuous set up translates to a balance relation on cells, i.e. one obtains

$$0 = \int_{\mathbf{C}} \operatorname{div} \tau \, \mathrm{d}x = \int_{\partial \mathbf{C}} n \cdot \tau \, \mathrm{d}l = \sum_{j=1}^{4} \int_{\mathbf{e}_j} n \cdot \tau \, \mathrm{d}l \approx \sum_{i=1}^{4} h_i f_i$$

where the discrete forces f_i for $i = 1, \ldots, 4$ are associated with the four edges $e_1, \ldots, e_4$ (numbered counter clock wise, starting with the upper edge, cf. Figure 3) of the cell $\mathbf{C}$ and h_i are the corresponding edge lengths. Thus, the discrete balance of forces reads as

$$0 = \sum_{i=1}^{4} h_i f_i \tag{4.1}$$

for all cells $\mathbf{C}$. Given the above numbering of the edges, the balance of torques turns into the equation

$$0 = (f_{1,1} + f_{4,1}) - (f_{2,2} + f_{3,2}) \tag{4.2}$$

for all cells $\mathbf{C}$, where $f_{i,j}$ is the jth component of the force vector f_i. Finally, the discrete boundary conditions are encoded as follows. We consider a piecewise constant force f for facets of subdomains on the boundary ∂D. These forces are then equally distributed on the edges of cells $\mathbf{C}$ touching ∂D on which $v = 1$. In explicit, given a subdomain D_i with a facet F on ∂D and an element E with $v = 1$ and an edge e_j on F, we define the force density

$$f_j = \frac{\int_F v \, \mathrm{d}l}{\int_F \mathrm{d}l} f \tag{4.3}$$

All the discrete counterparts of the conditions in (3.3) are assembled in a linear system $\mathbf{A}\mathbf{f} = \mathbf{b}$ for the vector of forces $\mathbf{f}$ on all edges. The matrix $\mathbf{A}$ and the right hand side $\mathbf{b}$ have the following block structure

$$\mathbf{A} = \begin{bmatrix} \mathbf{A}_f \\ \mathbf{A}_t \\ \mathbf{A}_{bc} \end{bmatrix}, \quad \mathbf{b} = \begin{bmatrix} 0 \\ 0 \\ \mathbf{b}_{bc} \end{bmatrix}.$$

Here, the index f refers to the force balance, the index t to the conservation of torque, and bc to the boundary condition. Now, solving the state equation coincides with minimizing the stored elastic energy

$$\mathbf{E} = \frac{1}{2} \sum_{\mathbf{C}} h^2 \sum_{i=1}^{4} \sum_{j=1}^{2} \frac{(f_{i,j}(\mathbf{C}))^2}{E}$$

with $f_i(\mathbf{C})$ denoting the force vectors on the edges of the cell $\mathbf{C}$, subject ot the constraint $\mathbf{A}\mathbf{f} = \mathbf{b}$. This can be rephrased in a Lagrangian formulation for the Lagrangian

$$\mathbf{L}(\mathbf{f}, \lambda) = \frac{1}{2} \mathbf{f}^T \mathbf{M} \mathbf{f} + \mathbf{f} \lambda^T (\mathbf{b} - \mathbf{A}\mathbf{f}) \, .$$

Due to the invertibility of the matrix $\mathbf{M}$ we obtain the equations

$$\begin{aligned} \mathbf{f} &= \mathbf{M}^{-1}\mathbf{A}^T\lambda \quad \text{and} \\ \mathbf{A}\mathbf{M}^{-1}\mathbf{A}^T\lambda &= \mathbf{b}\,. \end{aligned} \tag{4.4}$$

as the necessary conditions for a saddle point. They have to be solved first for the dual solution λ and then for the force vector $\mathbf{f}$. If $\ker\mathbf{A}^T = \{0\}$, then $\mathbf{Z} = \mathbf{A}\mathbf{M}^{-1}\mathbf{A}^T$ is positive definite and thus invertible. In general $\mathbf{A}^T$ is underdetermined with nontrivial kernel. Thus, we have to eliminate rows of $\mathbf{A}$ to reduce the kernel. For domains consisting of a single subdomain D_i with either periodic, branching periodic or non-periodic boundary conditions, the linear dependencies can be reduced to a small number of cases (cf. [11]). For composite domains consisting of several subdomains with different coupling and boundary conditions, the number, type and complexity of linear dependencies increases. Let us suppose that the number of boundary conditions (e.g. the number of edges on the boundary with prescribed forces is large enough to ensure that $\mathbf{A}^T$ has more rows than columns. Then, we apply a QR-decomposition of $\mathbf{A}^T$ to find a basis of its kernel and use this to reduce the linear system $\mathbf{A}\mathbf{f} = \mathbf{b}$ by the elimination of redundant equations. This in turn successively reduces $\mathbf{A}$ and $\mathbf{b}$ until A has full (column-)rank and thus $\ker\mathbf{A}^T = \{0\}$. For the results presented here the `CHOLMOD` [3] as a tool in the `Suitesparse` package was used, which comes along with an efficient parallel implementation.

5 Shape optimization

Optimization of the elastic shape coincides in the discrete set up with an optimization of the discrete phase field and thus a minimization of the objective functional (3.2) added up over all subdomains. To this end, we apply an alternating solution strategy, i.e. we alternatingly solve for the forces $\mathbf{f}$ for fixed discrete phase field $\mathbf{v}$ and improve the phase field v for given forces $\mathbf{f}$. A threshold for the difference between two consecutive phase fields in L^2 is taken into account as a stopping criterium for this descent scheme. To improve the discrete phase field given a force vector $\mathbf{f}$ we apply a Gauss-Seidel type iteration that optimizes the values of $\mathbf{v}$ on single cells of the finite volume mesh. Let us consider the discretized version of $\mathcal{J}$ given in (3.2)

$$\begin{aligned} \mathbf{J}[\mathbf{v}] &:= \min_{\tau\in\Sigma_{\text{ad}}} \sum_{\mathbf{C}} \mathbf{J}_{\mathbf{C}}[\mathbf{v}] \text{ with} \\ \mathbf{J}_{\mathbf{C}}[\mathbf{v}] &= \frac{|\sigma(\mathbf{C})|^2}{\mathbf{v}(\mathbf{C})} + \beta\mathbf{v}(\mathbf{C}) + \frac{\eta}{\epsilon}\frac{32}{\pi^2}(\mathbf{v}(\mathbf{C})-\delta)(1-\mathbf{v}(\mathbf{C})) \\ &\quad + \frac{\eta\epsilon}{4}\sum_{i=1}^{4}\frac{(\mathbf{v}(\mathbf{C})-\mathbf{v}(\mathbf{C}^{(i)}))^2}{h^2} \end{aligned}$$

Here, $\mathbf{C}^{(i)}$ denotes the cell adjacent to $\mathbf{C}$ across the edge $\mathbf{e}_i$. To find a minimum of $\mathbf{J}[\mathbf{v}]$ for $\mathbf{v}(\mathbf{C})$ for all $\mathbf{C}$ and for fixed $\mathbf{v}(\mathbf{C}^{(i)})$, we we apply Newton's method to compute the

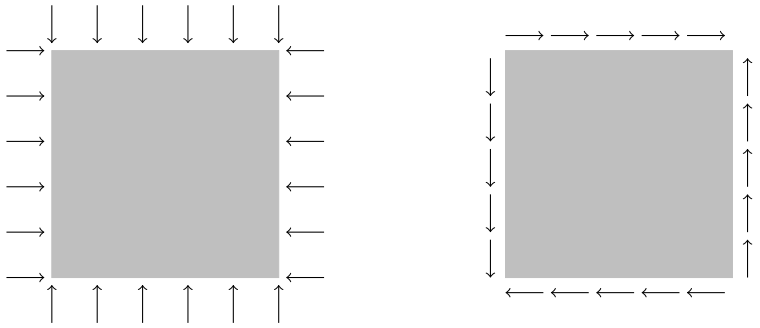

Figure 4: Sketch of the applied loads: Compression (left) and shear (right)

minimum of the rescaled function $\mathbf{v}(\mathbf{C}) \mapsto \mathbf{J}_{\mathbf{C}}(e^{-\mathbf{v}})$. The rescaling turns out to be an appropriate reformulation to overcome difficulties due to the singularity at $v(\mathbf{C}) = 0$.

To ensure a good performance of Newton's method, it is important to choose a suitable initialization of v. To this end we consider the local terms of the cost functional dropping the term involving the discrete gradient and define: $\tilde{\mathbf{J}}_{\mathbf{C}}(\mathbf{v}) = \frac{|\sigma|^2}{\mathbf{v}} + \beta\mathbf{v} + \frac{\eta}{\epsilon}\frac{32}{\pi^2}(\mathbf{v} - \delta)(1 - \mathbf{v})$. It is easy to check that this function has two minima and we initialize $\mathbf{v}$ with the minimal value of these two minima, again using in the algorithm the rescaled function $\mathbf{v}(\mathbf{C}) \mapsto \tilde{\mathbf{J}}_{\mathbf{C}}(e^{-\mathbf{v}})$ (or an approximation of it) as long as this value is smaller or equal 1. Otherwise, we initialize with the value 1. This led to an initialization $\mathbf{v}$ depending on the current stress value on $\mathbf{C}$. Starting from the second iteration of the alternating descent algorithm, the phase field could also be initialized using the result of the last phase field optimization. However, this approach is prone to becoming stuck in local minima.

6 Results

We applied our method for two different loads on a quadratic domain $D \subset [0, 1]^2$, subdivided into subdomain as displayed in Figure 2. In particular, the central region of the domain is filled with subdomains with inscribed locally periodic elastic structure and periodic boundary conditions for the forces, where as in the vicinity of the boundary branching periodic subdomains are taken into account. The two load scenarios are compression and shear as depicted in Figure 4.

For all domain types, the subdomains were discretized using $N \times N$ cells with $N = 200$. On each cell of the outer layer, forces were applied on the edge intervals $[\frac{2}{6}N, \frac{3}{6}N]$, $[\frac{4}{6}N, \frac{5}{6}N]$ on all horizontal and vertical boundaries. These forces are depicted in Figure 4 for both scenario.

Compression load: Pillar-like structures support the load on the boundary, branching structures transfer load to a mesh-like structure in the center region of the domain as depicted in Fig 5. The elastic structures on corner and coupling cells connect the branching periodic pillars. Let us point to a small artifact in the optimal shape shown

in one of the magnifications, where the phase field could obviously not been fully optimized locally.

Shear load: Fig 6 shows the optimal elastic shape in case of the shear load. On the resulting compound, optimized elastic structure forces are transferred via branching type structures to the center.

References

[1] Allaire, G. *Shape optimization by the homogenization method*, vol. 146 of *Applied Mathematical Sciences*. Springer-Verlag, New York, 2002.

[2] Bendsøe, M. P. *Optimization of structural topology, shape, and material*. Springer-Verlag, Berlin, 1995.

[3] Chen, Y., Davis, T. A., Hager, W. W., and Rajamanickam, S. Algorithm 887: Cholmod, supernodal sparse cholesky factorization and update/downdate. *ACM Trans. Math. Softw. 35*, 3 (Oct. 2008), 22:1–22:14.

[4] Cioranescu, D., and Donato, P. *An Introduction to Homogenization*. Oxford University Press, Oxford, 1999.

[5] E, W., and Engquist, B. The heterogeneous multiscale methods. *Commun. Math. Sci. 1*, 1 (2003), 87–132.

[6] E, W., and Engquist, B. The heterogeneous multi-scale method for homogenization problems. In *Multiscale Methods in Science and Engineering*, vol. 44 of *Lecture Notes in Computational Science and Engineering*. Springer Berlin Heidelberg, 2005, pp. 89–110.

[7] E, W., Engquist, B., and Huang, Z. Heterogeneous multiscale method: A general methodology for multiscale modeling. *Physical Review B 67*, 9 (March 2003), 1–4.

[8] E, W., Ming, P., and Zhang, P. Analysis of the heterogeneous multiscale method for elliptic homogenization problems. *J. Amer. Math. Soc. 18*, 1 (2005), 121–156.

[9] Kohn, R. V., and Wirth, B. Optimal fine-scale structures in compliance minimization for a uniaxial load. *Proceedings of the Royal Society of London A: Mathematical, Physical and Engineering Sciences 470*, 2170 (2014).

[10] Kohn, R. V., and Wirth, B. Optimal fine-scale structures in compliance minimization for a shear load. *Communications in Pure and Applied Mathematics* (2015). to appear.

[11] Lüthen, N. Numerical shape optimization of branching-periodic elastic structures. Master thesis, Univerisity of Bonn, 2016.

[12] Milton, G. W. *The Theory of Composites.* Cambridge University Press, 2002.

[13] Modica, L., and Mortola, S. Un esempio di Γ^--convergenza. *Boll. Un. Mat. Ital. B (5) 14*, 1 (1977), 285–299.

[14] Müller, R. Hierarchical microimaging of bone structure and function. *Nat. Rev. Rheumatol. 5*, 7 (2009), 373–381.

[15] Müller, V., Brylka, B., Dillenberger, F., Glöckner, R., and Böhlke, T. Homogenization of elastic properties of short-fiber reinforced composites based on microstructure data. *J. Compos. Mater. 50*, 3 (mar 2015), 297–312.

[16] Nemat-Nasser, S., Wills, J., Srivastava, A., and Amirkhizi, A. Homogenization of periodic elastic composites and locally resonant materials. *Phys. Rev. B 83* (Mar 2011), 104103.

[17] Penzler, P., Rumpf, M., and Wirth, B. A phase-field model for compliance shape optimization in nonlinear elasticity. *ESAIM: Control, Optimisation and Calculus of Variations 18*, 1 (2012), 229–258.

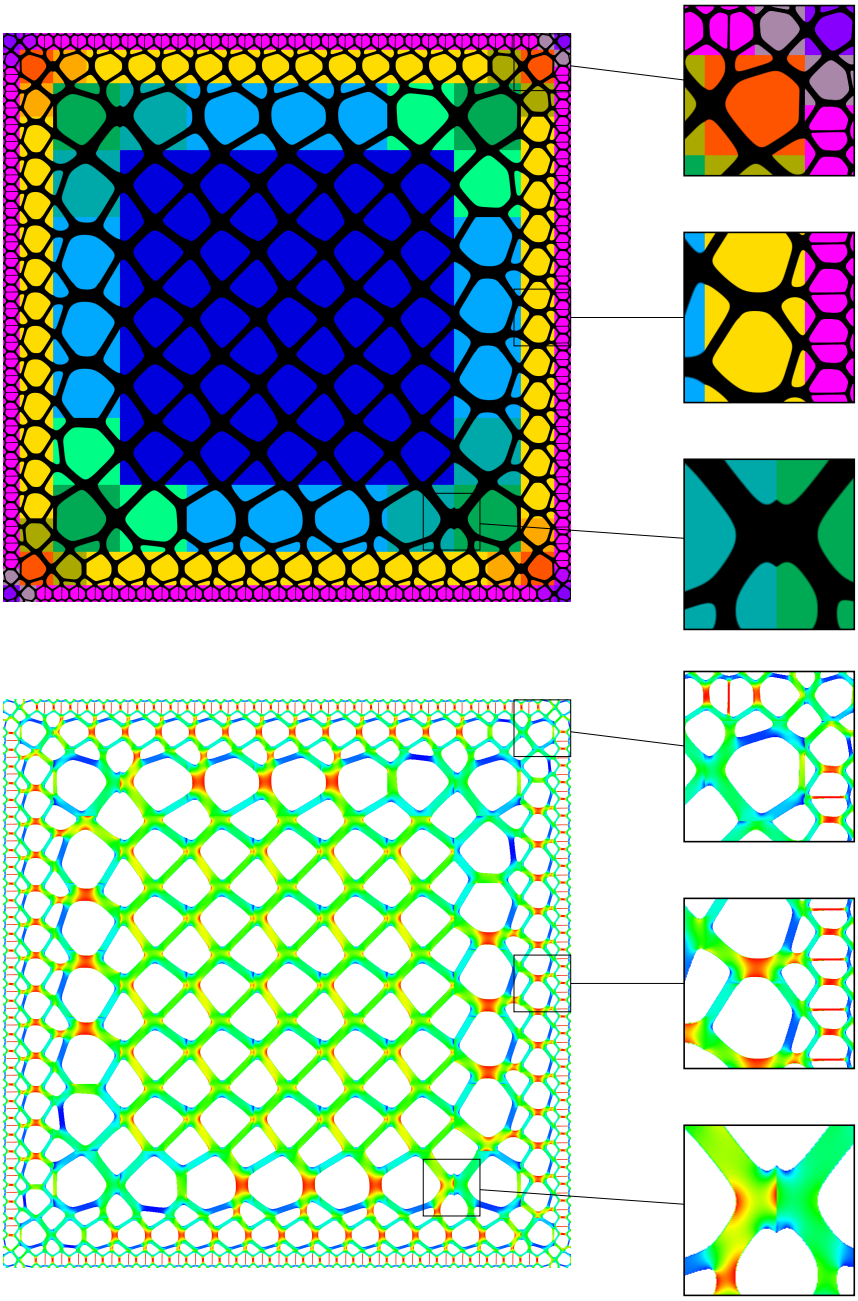

Figure 5: The optimal shape for the compression load case and a subdomain structure with 13 cell types is depicted (top). We show in addition a color coding of the von Mises stresses using the colorbar on the set $[\mathbf{v} > 0.5]$ (bottom).

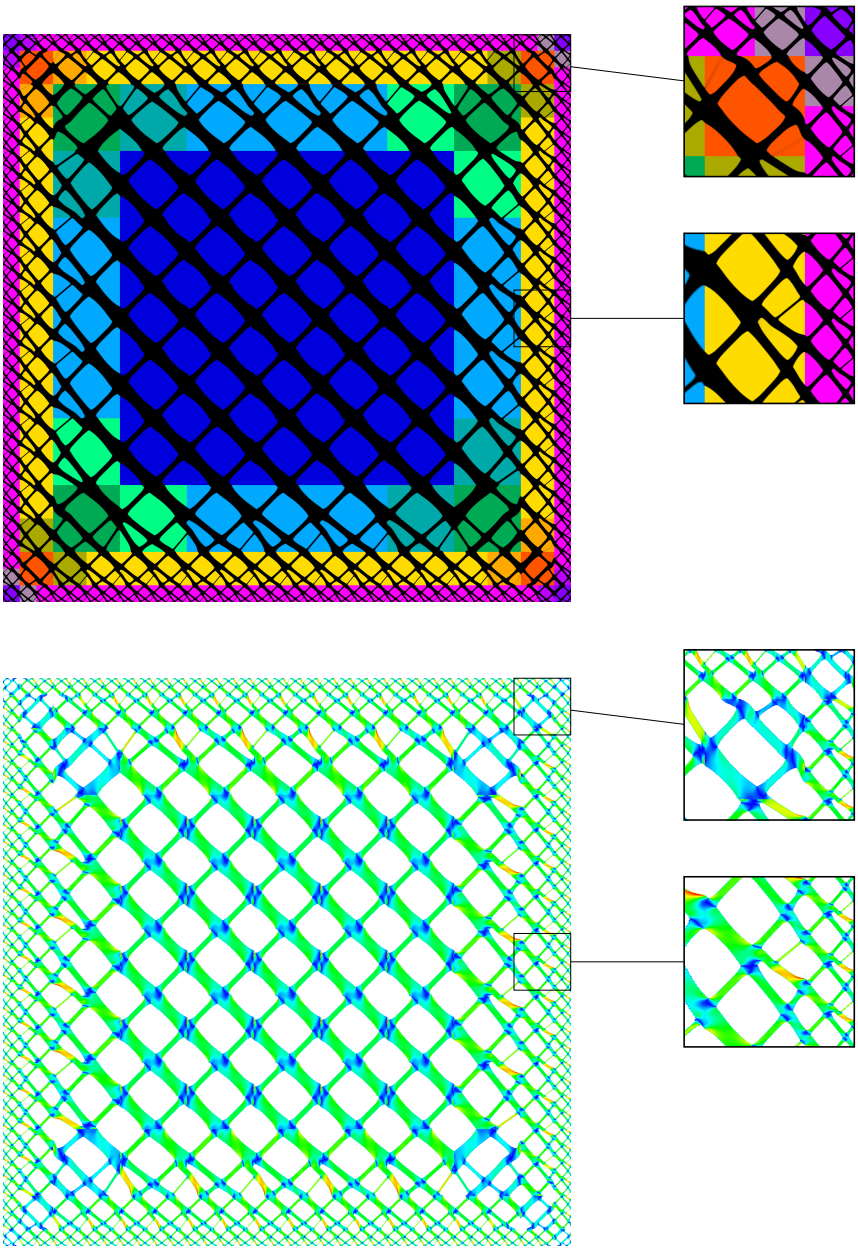

Figure 6: The optimal shape for the shear load case and the same subdomain structure as in Fig. 5 is displayed. with two regions being magnified on the right. Again together with the optimal shape (top) the associated von Mises stresses are rendered (bottom).